Ferroelectric switching assisted by laser illumination

Jiabin Chen,[1,2,3] Liangliang Hong,[1,2] Bing Huang,[3,4,*] and Hongjun Xiang[1,2,5,†]

[1]*Key Laboratory of Computational Physical Sciences (Ministry of Education), Institute of Computational Physical Sciences, State Key Laboratory of Surface Physics, and Department of Physics, Fudan University, Shanghai 200433, China*

[2]*Shanghai Qi Zhi Institute, Shanghai 200030, China*

[3]*Beijing Computational Science Research Center, Beijing 100193, China*

[4]*Department of Physics, Beijing Normal University, Beijing 100193, China*

[5]*Collaborative Innovation Center of Advanced Microstructures, Nanjing 210093, China*

(Received 16 September 2023; revised 26 December 2023; accepted 17 January 2024; published 4 March 2024)

We explore the fascinating dynamics of ferroelectric materials under illumination, which holds great potential to advance the field of optoferroelectricity. First, we introduce a general Hamiltonian-based model to explain how light exposure weakens ferroelectric polarity and reduces potential barriers in a ferroelectric system. Second, the properties and the dynamic evolution process of ferroelectric $BaTiO_3$ and SnTe under illumination are investigated using the first-principles methods, validating our model. The results demonstrate that illumination induces the redistribution of charge density and the reorganization of potential energy surface, thereby driving the transition from ferroelectric to paraelectric phases. Our findings reveal the potential for light-modulated ferroelectric memory and could propel the development of advanced ferroelectric devices. This study, therefore, represents a key step toward a comprehensive understanding of optoferroelectricity and its potential applications.

DOI: 10.1103/PhysRevB.109.094102

I. INTRODUCTION

Ferroelectric materials, characterized by spontaneous polarization, switchable electric dipoles, and ferroelectric-paraelectric phase transitions above the Curie temperature T_C [1], have garnered significant interest due to their promising applications in nonvolatile memory devices [2,3], pyroelectric sensors [4,5], piezoelectric actuators [6,7], and energy harvesting systems [8,9]. Nevertheless, the stability and reversibility of ferroelectricity present a formidable contradiction that demands attention. On one hand, the presence of high potential barriers in the material matrix is desirable for achieving elevated ferroelectric transition temperatures, which imparts superior thermal stability to the system. On the other hand, such high potential barriers necessitate a substantial electric field to reverse the ferroelectric polarization, leading to increased coercive forces and energy consumption. The resolution of this fundamental contradiction between stability and reversibility is of paramount importance for the optimization of ferroelectric devices.

Recent advancements in high-powered and ultrafast laser sources, combined with emerging detection techniques, have revolutionized the possibilities for precise control and manipulation of ferroelectric materials. Ultrafast optical inversion of ferroelectric polarization in $LiNbO_3$ was experimentally achieved through femtosecond midinfrared pulse resonance excitation [10]. The engineering of three-dimensional nonlinear photonic crystals has become a tangible reality through the full-optical polarization of ferroelectric domains using infrared femtosecond pulses [11,12]. Moreover, the quantum paraelectric-ferroelectric phase transitions in $SrTiO_3$ through the ingenious application of ultrashort terahertz pulses have been achieved [13,14], followed by a possible explanation from the perspective of phonon soft mode excitation [15]. These developments highlight the increasing relevance and potential of utilizing laser-assisted techniques in the investigation and manipulation of these complex ferroelectric materials.

In this study, using a simple Hamiltonian-based model, we propose that illumination can weaken the ferroelectric polarity and reduce the potential barrier of ferroelectric materials under the premise of an invariant lattice. To confirm this idea, using first-principles methods, including density functional theory (DFT) and real-time time-dependent density functional calculations (rt-TDDFT), we analyze the ground and excited state properties of bulk ferroelectric material $BaTiO_3$ and two-dimensional in-plane ferroelectric material SnTe. In our investigation of the dynamic evolution, it becomes evident that these two materials possess the capability to effectively reduce the ferroelectric potential barrier, attenuate the ferroelectric polarization, and potentially facilitate the transition from a ferroelectric to a paraelectric phase when subjected to illumination.

II. GENERAL THEORY

In order to explore the impact of light on the ferroelectric instability, we will analyze a linear $A1$-B-$A2$ model [16], where $A1$ and $A2$ are generally anions and B is generally cations. $A1$-B and B-$A2$ respectively represent two unequal

*bing.huang@csrc.ac.cn
†hxiang@fudan.edu.cn

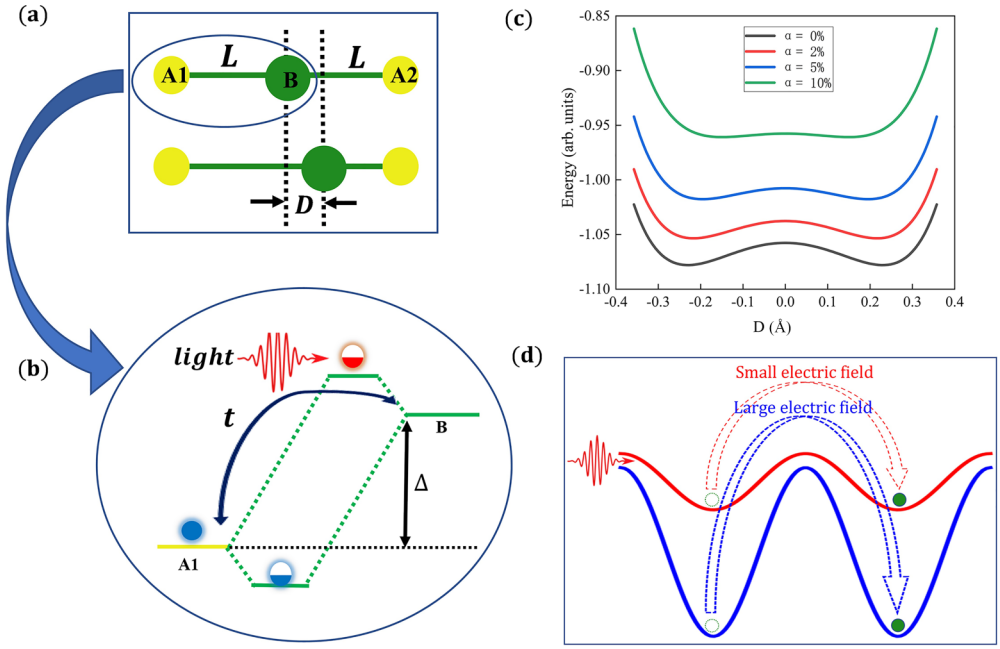

FIG. 1. (a) Schematic of the single-chain ferroelectric model where atom A represents a coordination atom and atom B signifies the displacement atom causing polarization within the ferroelectric material. (b) Depiction of the single-chain ferroelectric model Hamiltonian under light exposure, with t denoting the hopping integral between atoms A and B, and Δ expressing the energy difference between the orbital of atom A and B. (c) PES of the single-chain ferroelectric model as a function of the displacement of atom A. The blue, orange, green, and red lines correspond to the PES of the ground state and excited states with excitation rates of 2%, 5%, and 10% respectively. (d) Schematic diagram of achieving ferroelectric inversion using the synergistic effect between small electric fields and laser assistance.

bonds in ferroelectrics that cause ferroelectric polarization. The schematic representation of this model is delineated in Fig. 1(a). The total energy E_{tot} for the two-site system comprised of A and B sites is presented as follows:

$$E_{\text{tot}} = E_{\text{rep}} + E_{\text{hop}}.$$

Here, we use the term $E_{\text{rep}} = \frac{c_1}{(L+D)^{12}} + \frac{c_1}{(L-D)^{12}}$ $(c_1 > 0)$, a simplified form of the Lennard-Jones potential, to denote the total Pauli repulsion energy, where L is the original bond length of $A1$-B and B-$A2$ and D is the displacement of the B ion. Additionally, the terms E_{hop} represents the energy decrement caused by the hybridization between the unoccupied orbital of the B ion and the occupied orbital of the $A1/A2$ ion, as depicted in Fig. 1(b). Its expression can be inferred from the subsequent mean-field Hamiltonian; the electronic interaction Hamiltonian for the entire system can be expressed as follows:

$$H_{\text{hop}} = -t(a_1^+ a_2 + a_1^+ a_3 + \text{H.c.}) + \Delta/2(a_1^+ a_1 - a_2^+ a_2 - a_3^+ a_3),$$

where t represents the hopping integral and $\Delta(>0)$ is the energy difference between the empty orbital of B and the occupied orbital of $A1/A2$. By diagonalizing the Hamiltonian, we can obtain the hopping energy after considering the excitation of electrons E_{hop} as follows:

$$E_{\text{hop}} = \alpha\left(\sqrt{\frac{\Delta^2}{4} + 4(t_{B-A1})^2 + 4(t_{B-A2})^2} + \Delta\right) - \frac{\Delta}{2}.$$

Here, α represents the proportion of electrons excited by illumination. According to Harrison's method [17], the dependence of the hopping integral on the bond distance can be written as $t_{B-A1} = \frac{c_2}{(L+D)^2}$ and $t_{B-A2} = \frac{c_2}{(L-D)^2}(c_2 > 0)$. Therefore, E_{tot} can be expressed as

$$E_{\text{tot}} = \frac{c_1}{(L+D)^{12}} + \frac{c_1}{(L-D)^{12}} + \alpha\left(\sqrt{\frac{\Delta^2}{4} + 4\left(\frac{c_2}{(L+D)^2}\right)^2 + 4\left(\frac{c_2}{(L-D)^2}\right)^2} + \Delta\right) - \frac{\Delta}{2},$$

which is a function of the parameter D for various excitation electron ratios in the centrosymmetric linear model, i.e., potential energy surface (PES), as depicted in Fig. 1(c).

Through this qualitative model, two key conclusions can be drawn. First, it is evident that the total energy of the system increases with the proportion of excited electrons. This is because the electrons in the valence band absorb a certain frequency of light and transition to the conduction band under radiation, leading to an increase of the total energy of the system. Second, an interesting observation is that as the number of excited electrons increases, the ferroelectric polarization magnitude, along with the potential barrier, decreases and eventually disappears at a certain alpha. The competition between electron repulsion energy and hopping energy leads to the formation of two equivalent potential wells in the potential energy surface of the ferroelectric system, with the

intermediate atom occupying one of the wells and breaking the central inversion symmetry of the system, resulting in a local polarization. We assume that light only affects hybridization energy without repulsion energy, which is reasonable as the repulsion energy is mainly due to the overlap of the core electrons. Illumination reduces the energy lowering caused by orbital hybridization, thereby weakening the hopping interaction between electrons, making the jumping behavior of electrons between two lattice points less active. This gives the repulsion energy an advantage over the hopping energy, thereby altering the potential energy curve of the system's total energy. When the number of excited electrons reaches a critical proportion, the energy reaches its lowest point at $D = 0$, meaning that there is no longer any ferroelectric instability and a transition from ferroelectric to paraelectric occurs. An alternative interpretation emerges from the total energy evolution. In general, it is observed that the band gap of the ferroelectric phase is larger than that of the paraelectric phase. This difference engenders a greater energy increase in the ferroelectric phase than in the paraelectric phase when the same number of electrons are excited. As a consequence, the material exhibits a distinct tendency to transition from ferroelectric stability to paraelectric stability [18].

By the proposed model, we present an approach that combines a small electric field with laser assistance to achieve ferroelectric inversion. The procedure involves initially using a laser to lower the ferroelectric potential barrier and subsequently employing a small electric field to induce the ferroelectric switching. Note that the depolarizing field may hinder the polarization switching in experiment. Following the cooling and relaxation process, the system returns to its original high potential barrier state, but with a reversed polarization direction. This proposed technique allows for ferroelectric switching to be achieved using a small electric field instead of the conventionally required large electric fields, as illustrated in Fig. 1(d). By harnessing the capabilities of laser-manipulated ferroelectric order parameters, we overcome the challenges posed by high potential barriers while ensuring the stability and reversibility of ferroelectricity. This method holds immense promise in advancing the field of ferroelectric research and sets the stage for the design of cutting-edge ferroelectric devices.

III. METHOD

We performed calculations on the ground-state properties using the Vienna Ab initio Simulation Package (VASP) [19]. In our simulations, we employed an energy cutoff of 500 eV for the expansion of wave functions into a plane wave basis set. This value was chosen following meticulous convergence tests to ensure the accuracy and reliability of the results. We utilized the constrained DFT method [20] to compute the atomic forces when electrons are excited to the conduction band under illumination. Moreover, we performed real-time time-dependent density functional theory (rt-TDDFT) simulations [21] within the framework of density functional theory (DFT) based on norm-conserving pseudopotentials [22] and the Perdew-Burke-Ernzerhof functional [23]. We used a plane wave nonlocal pseudopotential Hamiltonian, which is implemented in the PWmat code [24]. The wave functions were expanded onto a plane wave basis set with an energy cutoff of 50 Rydberg. In the real-time TDDFT simulations, we employed the *NVE* ensemble and used a 64-atom supercell for both $BaTiO_3$ and SnTe, sampling the Brillouin zone at the Γ point. The time step was set to 0.1 fs. The duration of laser pulses is $\sqrt{2}\sigma = 12$ fs, with photon energies of 2.37 and 3.1 eV for $BaTiO_3$ and SnTe respectively. We set the peak of the light at 30 fs both for $BaTiO_3$ and SnTe.

IV. CASE OF A BULK FERROELECTRICITY: $BaTiO_3$

$BaTiO_3$ is a widely studied perovskite material, renowned for its exceptional dielectric [25,26], piezoelectric [27], and ferroelectric properties. Since its discovery in the 1940s, $BaTiO_3$ has garnered immense attention from academia and industry, thanks to its extensive applications in capacitors, sensors, actuators, transducers, and memory devices. The phase transition temperature of $BaTiO_3$ is around 396 K [28], where the material undergoes a phase transition from a tetragonal ferroelectric phase to a cubic nonferroelectric phase associated with crystal structural distortions [29]. The high-temperature cubic phase consists of regular corner-sharing octahedral TiO_6 units that define a cube with Ti vertices and Ti-O1-Ti edges. Ba^{2+} is located at the center of the cube with a nominal coordination number of 12. Lower symmetry phases are stabilized at lower temperatures and involve movement of the Ti^{4+} to off-center positions. The remarkable properties of this material arise from the cooperative behavior of the Ti^{4+} distortions [30].

In terms of our model, the *A* atom is considered as the O1 of $BaTiO_3$, while *B* represents the Ti atoms. Before illumination, owing to its ferroelectric nature, the Ti atom resides in one of the potential wells of its ferroelectric potential surface, resulting in unequal bond lengths with the two O1 atoms above and below the Ti site. We use constrained DFT under static conditions to simulate the electron excitation caused by illumination with a $3 \times 3 \times 3$ supercell. Fig. 2(b) depicts an image extracted from one unit cell, displaying the real-space charge density difference (CDD) after the excitation of 0.375% of the total valence electrons, which shows that the positively charged Ti^{4+} ions are attracted to the electron group beneath, generating a downward force along the z axis. Here, CDD $= \rho$(excited state)$-\rho$(ground state). The negatively charged O^{2-} ions are repelled by the electron group beneath, producing an upward force along the z axis. The magnitudes and directions of these forces can be observed from Fig. 2(c). The electrons transfer from the vicinity of the Ti atom and accumulate beneath the O1 and Ti atoms, which is consistent with a previous report [31]. This information can also be extracted from the density of states (DOS) plot in Fig. 1(e). The red (black) dashed lines represent the state density before illumination, while the red (black) solid lines depict the state density 150 fs postillumination. The orange and green areas represent the excited electrons and holes, respectively. A strong laser pulse pumps electrons from the $2p$ orbital of oxygen to the $3d$ orbital of titanium, altering the potential surface of $BaTiO_3$. This leads to a redistribution of ferroelectric charge density from the original state, initiating highly directional ionic motion that drives the O1 atom

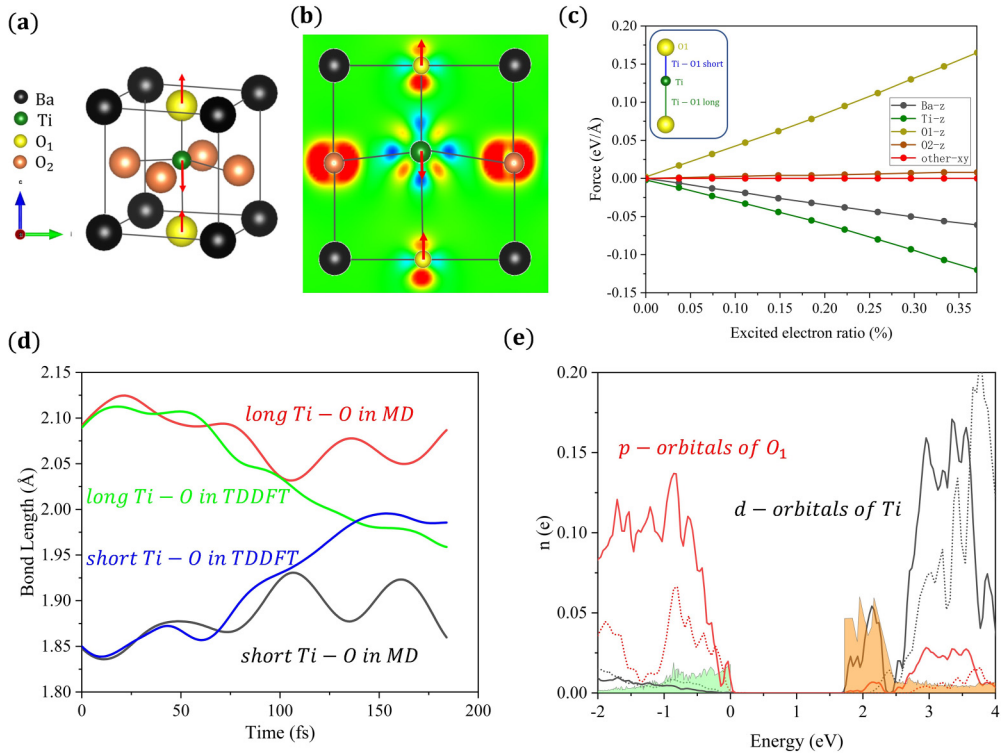

FIG. 2. (a) Crystal structure of $BaTiO_3$ in its ferroelectric phase. (b) CDD of $BaTiO_3$ after exciting 0.375% of total valence electrons. The red arrow indicates the direction of the force on the atom (c) Magnitude and direction of forces acting on each atom in $BaTiO_3$ after exciting 0.375% of total valence electrons. (d) The green and blue solid lines represent the time evolution of the long and short Ti-O bonds responsible for ferroelectric polarization, respectively, under ultrafast laser irradiation. The red and black solid lines represent the time evolution of the long and short Ti-O bonds responsible for ferroelectric polarization, respectively, obtained using the NVT ensemble in regular molecular dynamics simulations at the same temperature after laser heating. (e) Electronic density of states for $BaTiO_3$ in the ground state and excited state. The red (black) dotted line represents the density of states of O1 p orbitals (Ti d orbitals) before lighting, while the red (black) solid line represents the density of states of O1 p orbitals (Ti d orbitals) after 150 fs light pulse is applied. The orange and green regions represent the excited electrons and holes, respectively.

upwards and the Ti ion downwards, this phenomenon is consistent with the theory we mentioned earlier. Importantly, the transfer of electrons does not disrupt the symmetry within the *x*-*y* plane of the system. Laser irradiation induces a weakening of the Ti-O bond and pseudo Jahn Teller effect, enhancing the tendency towards the transition from polar structures to higher symmetric structures [31,32].

Further dynamical validation was conducted using rt-TDDFT. As shown in Fig. 2(d), we capture the temporal evolution of each bond length in $BaTiO_3$ under light excitation. The ferroelectric phase of $BaTiO_3$, characterized by long (and short) bond lengths initially, transitions to the state with almost equal bond lengths approximately 150 fs after the application of the light pulse. This indicates a structural phase transition of $BaTiO_3$ from the ferroelectric to the paraelectric phase, due to the transfer of energy from the photoexcited electrons to the lattice, resulting in a reorganization of the crystal potential surface. We also observe that the band gap width postillumination is slightly narrower than preillumination, which is also consistent with the conclusion that the band gap width of the paraelectric phase of $BaTiO_3$ is slightly smaller than that of the ferroelectric phase [29,33]. Following the light pulse, the long Ti-O1 bond shortens, while the short Ti-O1 bond lengthens. This is accompanied by a degree of oscillation but does not revert to the original size. This oscillation arises from the inertia of the atoms during the dynamical process and a reduction in the ferroelectric potential barrier as depicted in Fig. 2(b).

V. CASE OF A VDW FERROELECTRICITY: SnTe

The ferroelectric transition temperature of a monolayer SnTe film is dramatically elevated from the bulk material's 98b K to an impressive 270 K [34]; it has been theoretically demonstrated that the 0-K energy barrier for the polarization switching in SnTe thin films is higher than that in bulk SnTe when the thickness is larger than 2 unit cells (UCs), due to the competition between hybridization and Pauli repulsion interactions, and the 5-UC SnTe film has the largest energy barrier [35,36]. Fig. 3(a) shows the crystal structure of a monolayer SnTe thin film. This hallmark feature positions SnTe thin films as a potent contender in addressing the miniaturization challenges in ferroelectric devices. In a deeper exploration of the subject from both the modeling and dynamical evolution perspectives, we expand upon previous evidence that strong coupling between terahertz lasers and transverse optical phonon modes can trigger ferroic order switching in

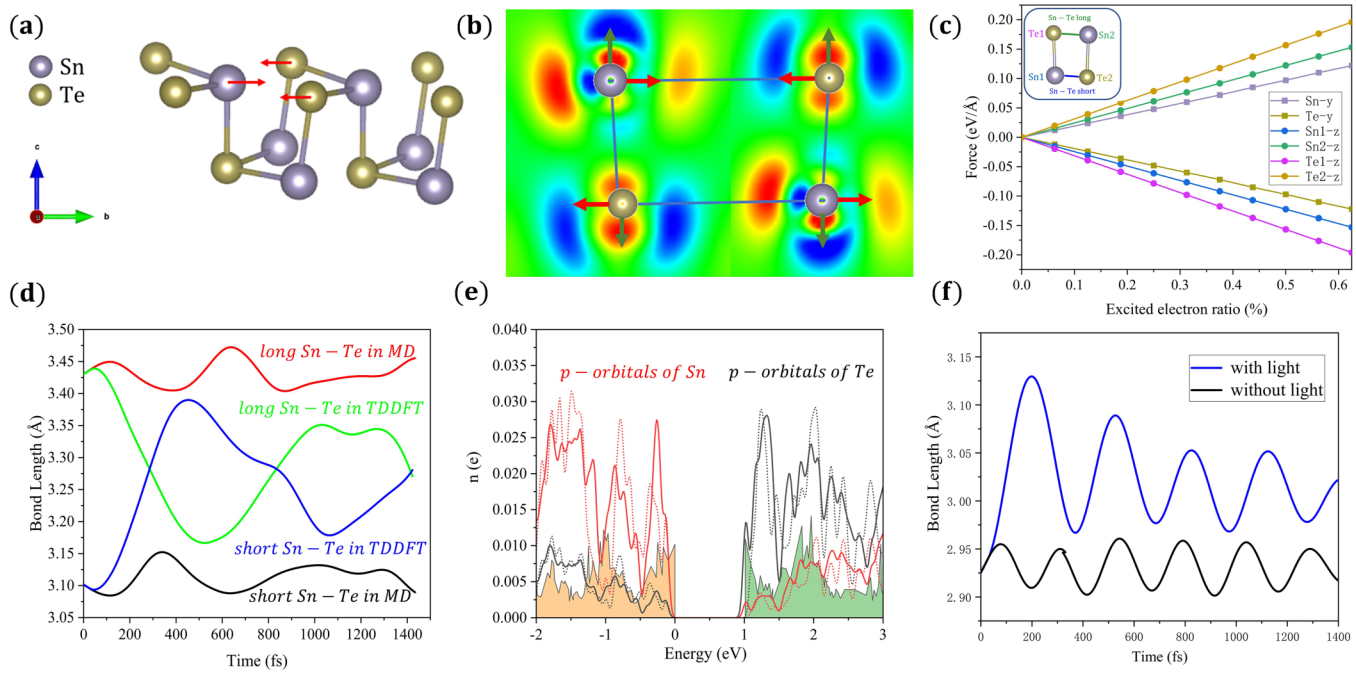

FIG. 3. (a) Crystal structure of SnTe in its ferroelectric phase. (b) CDD of SnTe after exciting 0.625% of electrons. The red arrow indicates the direction of the force on the atom. (c) Magnitude and direction of forces acting on each atom in SnTe after exciting 0.625% of electrons. (d) The green and blue solid lines represent the time evolution of the long and short Sn-Te bonds responsible for ferroelectric polarization, respectively, under ultrafast laser irradiation. The red and black solid lines represent the time evolution of the long and short Sn-Te bonds responsible for ferroelectric polarization, respectively, obtained using the NVT ensemble in regular molecular dynamics simulations at the same temperature after laser heating. (e) Electronic density of states for SnTe in the ground state and excited state. The red (black) dotted line represents the density of states of Sn (Te) p orbitals before lighting, while the red (black) solid line represents the density of states of Sn (Te) p orbitals after 2000 fs light pulse is applied. The orange and green regions represent the excited electrons and holes, respectively. (f) Temporal evolution of the z-direction Sn-Te bond, with blue indicating the presence of light and black indicating the absence of light. After illumination, the Sn-Te bond in the z-direction becomes longer.

SnTe, originally proven from the perspective of optical polarizability [31].

Our model is based on a configuration where Sn and Te are referred to as A and B atoms respectively. Owing to the equivalence of the Sn-Te-Sn chains along the [110] and [1$\bar{1}$0] directions, there is no polarization in the x direction, with ferroelectric polarity solely exhibited in the y direction. Upon exciting 0.625% of the electrons, as shown in Fig. 3(b), the positively charged Sn^{2+} ions experience a strong repulsion in the positive y direction due to the adjacent hole group. Concurrently, the negatively charged Te^{2-} ions are repelled in the negative y direction by the adjacent electron group. The magnitude and direction of these forces can be inferred from Fig. 3(c) as well.

As demonstrated in Fig. 3(e), laser pulses pump electrons from the p orbitals of Sn onto the p orbitals of Te, altering the potential energy surface of SnTe. This results in an inversion of the ferroelectric charge density from its original state, prompting the Sn-Te bonds inclined in the z direction to realign. Additionally, similar to $BaTiO_3$, the band gap width of SnTe marginally decreases after illumination. The rt-TDDFT calculations in Fig. 3(d) further confirm our model's conclusions. Postillumination, the length of the Sn-Te bonds oscillates over time, shortening for the long bonds and lengthening for the short ones, without reverting to their original sizes. This attests to a reduction in the ferroelectric polarity in the y direction, consequently weakening the ferroelectric potential barrier.

VI. DISCUSSION

The surface or interface effects of two-dimensional materials are non-negligible. Unlike $BaTiO_3$, where the force experienced by the atoms in the xy plane under light excitation is weak and does not alter its symmetry [as shown in Fig. 2(c)], the length of the Sn-Te bond along the z axis in SnTe elongates, as observed in Fig. 3(f). This elongation can be attributed to the hybridization of the p orbitals in Sn and Te, which results from carrier excitation induced by illumination. Consequently, the energy levels of the bonding state are elevated, while the energy levels of the antibonding state are reduced. In real space, this results in bond stretching to decrease the total energy. While this stretching force should ideally be isotropic and uniform, the broken spatial translation symmetry along the z axis in two-dimensional materials prevents its cancellation. In Fig. 3(b), CDD also shows that Sn is attracted by the external electron group and Te by the external hole group, both exerting a strong force outward from the plane. The magnitude and direction of these forces, as depicted in Fig. 3(c), imply that under illumination, the Sn-Te bond in the z direction will tend to increase along the z axis.

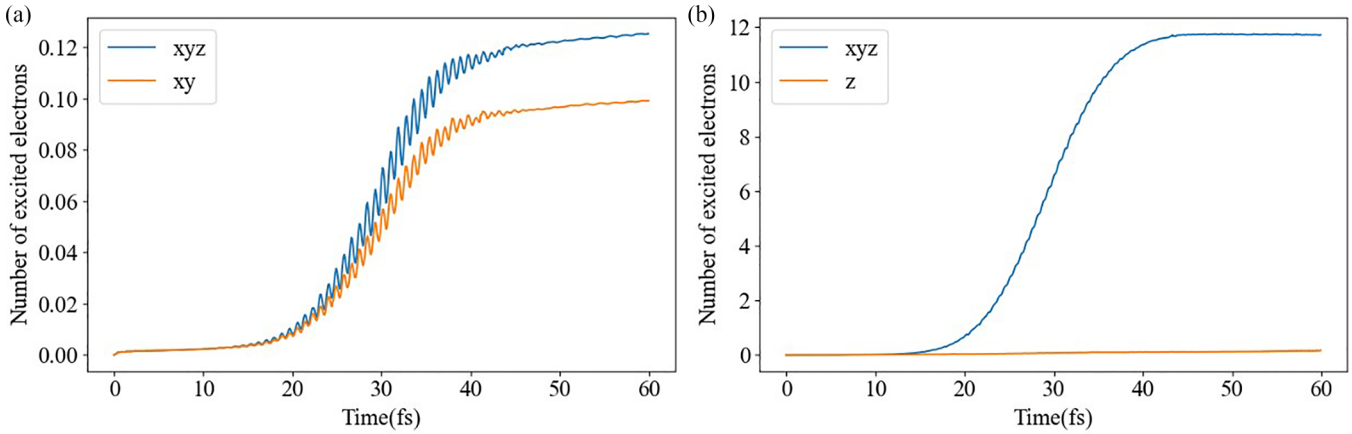

FIG. 4. (a) The time evolution of the number of excited electrons in $BaTiO_3$ following the application of laser polarization in the xyz direction (xy direction) is illustrated by the blue solid line (orange solid line). (b) The time evolution of the number of excited electrons in SnTe following the application of laser polarization in the xyz direction (z direction) is illustrated by the blue solid line (orange solid line).

In the *NVE* ensemble, excess energy is transferred to the cold lattice from hot carriers via electron-phonon coupling, thereby raising the system temperature. To eliminate the influence of temperature, we first determine the stable temperature after ultrafast laser, then we conduct molecular dynamics simulations at the same temperature using the *NVT* ensemble, as indicated by the red line and the black line in Figs. 2(d) and 3(d). Our simulations indicate that, at this temperature, the ferroelectric polarization does not exhibit a substantial decrease, indicating that light plays a predominant role in promoting ferroelectric phase transition.

In addition, we investigated the influence of photon frequency, photon fluence, and light polarization on the polarization intensity of ferroelectric materials. Our observations indicated that as the photon fluence increases, the ferroelectric-to-paraelectric phase transition in $BaTiO_3$ occurs more rapidly [see Fig. S1(a) of the Supplemental Material [37]]. This is reflected in the negative correlation between the time it takes for the long and short bonds to reach the crossover point and the increase in photon fluence. A higher photon fluence leads to the excitation of more electrons [see Fig. S2(a) of the Supplemental Material [37]], but it also causes more intense oscillations in bond lengths, consequently, the long and short bonds return to positions of higher ferroelectric polarization after the crossing over. The evolution of ferroelectric polarization with photon frequency follows a trend similar to that observed with photon flux. It is noted that, with an increase in photon energy, the required time for the phase transition progressively decreases [see Fig. S1(b) of the Supplemental Material]. This phenomenon is attributed to the ability of higher energy photons to excite electrons from lower energy levels in the valence band to the conduction band, which leads to a greater number of excited electrons [see Fig. S2(b) of the Supplemental Material]. Both of these factors act by influencing the quantity of excited electrons, thereby impacting the rate of the phase transition.

Considering the inherent ferroelectric polarity of $BaTiO_3$ in the z direction, we found that when the material is irradiated with a light field polarized solely in the xy plane while keeping other conditions constant, there is no significant change in the ferroelectric polarity of $BaTiO_3$ [see Fig. S3(a) of the Supplemental Material]. This can be attributed to the fact that the line connecting the real-space projections of the O p orbitals and Ti d orbitals lies along the z direction. Consequently, the absence of an electric field in the z direction hinders the excitation of O p-orbital electrons to the Ti d orbitals [see Fig. 4(a)]. Similarly, in the case of ferroelectric SnTe with polarity in the y direction, when it is irradiated with light polarized solely in the z direction, the ferroelectric polarity also remains nearly unchanged [see Fig. S3(b) of the Supplemental Material]. This is due to the fact that the line connecting the real-space projections of the Sn p orbitals and Te d orbitals lies along the y direction. Hence, the absence of an electric field in the y direction significantly hampers the excitation of Sn p-orbital electrons to the Te d orbitals. When only the nonpolarized light field is incident, few electrons are excited, whereas the presence of a ferroelectric polarization direction electric field can significantly increase the number of electron excitations [see Fig. 4(b)].

To investigate the damaging effect of laser on the material, we calculate the radial distribution functions, as shown in Fig. S4 of the Supplemental Material. The results indicate that, with the laser parameters of $F = 70\,\mathrm{mJ/cm^2}$ and $E_0 = 0.01$ Ha/Bohr, $BaTiO_3$ is approaching the melting point. In this case, the average rate of energy transfer is approximately 0.007 11 eV/fs per atom.

VII. SUMMARY

This study proposes a model for understanding the effect of light on ferroelectric materials, revealing that illumination weakens the ferroelectric polarity and reduces the potential barrier of these materials. This model was further demonstrated through first-principles methods applied to two different materials $BaTiO_3$ and SnTe. The findings suggest that using light can improve the control of ferroelectric polarization, potentially enabling more advanced applications in memory devices, sensors, and energy harvesting systems. The study also revealed the behavior of these materials under

illumination, specifically the transition from ferroelectric to paraelectric states. This could pave the way for innovative approaches to manipulate ferroelectric materials and contribute to the development of light-modulated ferroelectric memory. Moreover, the research investigated the properties of $BaTiO_3$ and SnTe under illumination, providing insights for their practical applications.

ACKNOWLEDGMENTS

The work at Fudan was supported by the National Key R&D Program of China (Grant No. 2022YFA1402901), NSFC (Grants No. 11825403, No. 11991061, and No. 12188101), and the Guangdong Major Project of the Basic and Applied Basic Research (Future functional materials under extreme conditions, Project No. 2021B0301030005).

[1] N. Setter, D. Damjanovic, L. Eng, G. Fox, S. Gevorgian, S. Hong, A. Kingon, H. Kohlstedt, N. Y. Park, G. B. Stephenson, I. Stolitchnov, A. K. Taganstev, D. V. Taylor, T. Yamada, and S. Streiffer, Ferroelectric thin films: Review of materials, properties, and applications, J. Appl. Phys. **100**, 051606 (2006).

[2] R. Guo, L. You, Y. Zhou, Z. Shiuh Lim, X. Zou, L. Chen, R. Ramesh, and J. Wang, Non-volatile memory based on the ferroelectric photovoltaic effect, Nat. Commun. **4**, 1990 (2013).

[3] A. Q. Jiang, W. P. Geng, P. Lv, J. Hong, J. Jiang, C. Wang, X. J. Chai, J. W. Lian, Y. Zhang, R. Huang, D. W. Zhang, J. F. Scott, and C. S. Hwang, Ferroelectric domain wall memory with embedded selector realized in $LiNbO_3$ single crystals integrated on Si wafers, Nat. Mater. **19**, 1188 (2020).

[4] Y. Chen, Y. Zhang, F. Yuan, F. Ding, and O. G. Schmidt, A Flexible PMN-PT Ribbon-based piezoelectric-pyroelectric hybrid generator for human-activity energy harvesting and monitoring, Adv. Electron. Mater. **3**, 1600540 (2017).

[5] E. Meirzadeh, D. V. Christensen, E. Makagon, H. Cohen, I. Rosenhek-Goldian, E. H. Morales, A. Bhowmik, J. M. G. Lastra, A. M. Rappe, D. Ehre, M. Lahav, N. Pryds, and I. Lubomirsky, Surface pyroelectricity in cubic $SrTiO_3$, Adv. Mater. **31**, 1904733 (2019).

[6] Y. Zhan, Y. Chen, M. Mietschke, L. Zhang, F. Yuan, S. Abel, R. Hühne, K. Nielsch, J. Fompeyrine, F. Ding, and O. G. Schmidt, Monolithically integrated microelectromechanical systems for on-chip strain engineering of quantum dots, Nano Lett. **16**, 5785 (2016).

[7] D. Zhou, N. Wang, T. Yang, L. Wang, X. Cao, and Z. L. Wang, A piezoelectric nanogenerator promotes highly stretchable and self-chargeable supercapacitors, Mater. Horiz. **7**, 2158 (2020).

[8] X. Wei, N. Domingo, Y. Sun, N. Balke, R. E. Dunin-Borkowski, and J. Mayer, Progress on emerging ferroelectric materials for energy harvesting, storage and conversion, Adv. Energy Mater. **12**, 2201199 (2022).

[9] C. R. Bowen, H. A. Kim, P. M. Weaver, and S. Dunn, Piezoelectric and ferroelectric materials and structures for energy harvesting applications, Energy Environ. Sci. **7**, 25 (2014).

[10] R. Mankowsky, A. Von Hoegen, M. Först, and A. Cavalleri, Ultrafast reversal of the ferroelectric polarization, Phys. Rev. Lett. **118**, 197601 (2017).

[11] X. Chen, P. Karpinski, V. Shvedov, K. Koynov, B. Wang, J. Trull, C. Cojocaru, W. Krolikowski, and Y. Sheng, Ferroelectric domain engineering by focused infrared femtosecond pulses, Appl. Phys. Lett. **107**, 141102 (2015).

[12] T. Xu, K. Switkowski, X. Chen, S. Liu, K. Koynov, H. Yu, H. Zhang, J. Wang, Y. Sheng, and W. Krolikowski, Three-dimensional nonlinear photonic crystal in ferroelectric barium calcium titanate, Nature Photon **12**, 591 (2018).

[13] T. F. Nova, A. S. Disa, M. Fechner, and A. Cavalleri, Metastable ferroelectricity in optically strained $SrTiO_3$, Science **364**, 1075 (2019).

[14] I. Katayama, H. Aoki, J. Takeda, H. Shimosato, M. Ashida, R. Kinjo, I. Kawayama, M. Tonouchi, M. Nagai, and K. Tanaka, Ferroelectric soft mode in a $SrTiO_3$ thin film impulsively driven to the anharmonic regime using intense picosecond terahertz pulses, Phys. Rev. Lett. **108**, 097401 (2012).

[15] C. Song, Q. Yang, X. Liu, H. Zhao, C. Zhang, and S. Meng, Electronic origin of laser-induced ferroelectricity in $SrTiO_3$, J. Phys. Chem. Lett. **14**, 576 (2023).

[16] H. Wei, Y. Yang, S. Chen, and H. J. Xiang, Lead-Free hybrid perovskite $N(CH_3)_4SnI_3$ with robust ferroelectricity induced by large and Non-Polar $N(CH_3)_4^+$ molecular cation, Nat. Commun. **12**, 637 (2021).

[17] W. A. Harrison, Tight-binding methods, Surf. Sci. **299–300**, 298 (1994).

[18] J. Chen, Y. Li, H. Yu, Y. Yang, H. Jin, B. Huang, and H. Xiang, Light-induced magnetic phase transition in van der Waals antiferromagnets, Sci. China Phys. Mech. Astron. **66**, 277511 (2023).

[19] G. Kresse and J. Furthmüller, Efficient iterative schemes for *ab initio* total-energy calculations using a plane-wave basis set, Phys. Rev. B **54**, 11169 (1996).

[20] C. Paillard, S. Prosandeev, and L. Bellaiche, *Ab initio* approach to photostriction in classical ferroelectric materials, Phys. Rev. B **96**, 045205 (2017).

[21] Z. Wang, S.-S. Li, and L.-W. Wang, Efficient real-time time-dependent density functional theory method and its application to a collision of an ion with a 2D material, Phys. Rev. Lett. **114**, 063004 (2015).

[22] D. R. Hamann, Optimized norm-conserving Vanderbilt pseudopotentials, Phys. Rev. B **88**, 085117 (2013).

[23] J. P. Perdew, K. Burke, and M. Ernzerhof, Generalized gradient approximation made simple, Phys. Rev. Lett. **77**, 3865 (1996).

[24] A. Raza, C. Hong, X. Wang, A. Kumar, C. R. Shelton, and B. M. Wong, NIC-CAGE: An open-source software package for predicting optimal control fields in photo-excited chemical systems, Comput. Phys. Commun. **258**, 107541 (2021).

[25] F. Wan, J. Han, and Z. Zhu, Dielectric response in ferroelectric $BaTiO_3$, Phys. Lett. A **372**, 2137 (2008).

[26] T. Zhou, J.-W. Zha, R.-Y. Cui, B.-H. Fan, J.-K. Yuan, and Z.-M. Dang, Improving dielectric properties of $BaTiO_3$/Ferroelectric polymer composites by employing surface hydroxylated $BaTiO_3$ nanoparticles, ACS Appl. Mater. Interfaces **3**, 2184 (2011).

[27] M. Acosta, N. Novak, V. Rojas, S. Patel, R. Vaish, J. Koruza, G. A. Rossetti, and J. Rödel, $BaTiO_3$-Based piezoelectrics:

fundamentals, current status, and perspectives, Appl. Phys. Rev. **4**, 041305 (2017).

[28] K. Sakayori, Y. Matsui, H. Abe, E. Nakamura, M. Kenmoku, T. Hara, D. Ishikawa, A. Kokubu, K. Hirota, and T. I. T. Ikeda, Curie temperature of $BaTiO_3$, Japan. J. Appl. Phys. **34**, 5443 (1995).

[29] M. B. Smith, K. Page, T. Siegrist, P. L. Redmond, E. C. Walter, R. Seshadri, L. E. Brus, and M. L. Steigerwald, Crystal structure and the paraelectric-to-ferroelectric phase transition of nanoscale $BaTiO_3$, J. Am. Chem. Soc. **130**, 6955 (2008).

[30] M. Gaudon, Out-of-Centre distortions around an octahedrally coordinated Ti^{4+} in $BaTiO_3$, Polyhedron **88**, 6 (2015).

[31] C. Lian, Z. A. Ali, H. Kwon, and B. M. Wong, Indirect but efficient: Laser-excited electrons can drive ultrafast polarization switching in ferroelectric materials, J. Phys. Chem. Lett. **10**, 3402 (2019).

[32] V. Polinger, P. Garcia-Fernandez, and I. B. Bersuker, Pseudo Jahn–Teller origin of ferroelectric instability in $BaTiO_3$ type perovskites: The Green's function approach and beyond, Phys. B (Amsterdam, Neth.) **457**, 296 (2015).

[33] S. Sanna, C. Thierfelder, S. Wippermann, T. P. Sinha, and W. G. Schmidt, Barium titanate ground- and excited-state properties from first-principles calculations, Phys. Rev. B **83**, 054112 (2011).

[34] K. Chang, J. Liu, H. Lin, N. Wang, K. Zhao, A. Zhang, F. Jin, Y. Zhong, X. Hu, W. Duan, Q. Zhang, L. Fu, Q. Xue, X. Chen, and S. H. Ji, Discovery of robust in-plane ferroelectricity in atomic-thick SnTe, Science **353**, 274 (2016).

[35] K. Liu, J. Lu, S. Picozzi, L. Bellaiche, and H. Xiang, Intrinsic origin of enhancement of ferroelectricity in SnTe ultrathin films, Phys. Rev. Lett. **121**, 027601 (2018).

[36] J. Zhou and S. Zhang, Terahertz optics-driven phase transition in two-dimensional multiferroics, Npj 2D Mater Appl **5**, 16 (2021).

[37] See Supplemental Material at http://link.aps.org/supplemental/10.1103/PhysRevB.109.094102 for the effect of different laser fluence and photon energy on ferroelectric polarization; The effect of different polarization of laser on ferroelectric polarization; Damage analysis under strong light conditions.